Polymer 50 (2009) 6091–6099

Contents lists available at ScienceDirect

Polymer

journal homepage: www.elsevier.com/locate/polymer

Network structures and dynamics of dry and swollen poly(acrylate)s. Characterization of high- and low-frequency motions as revealed by suppressed or recovered intensities (SRI) analysis of ^{13}C NMR

Yuko Miwa [a,*], Hiroyuki Ishida [a], Hazime Saitô [b,**], Masaru Tanaka [c], Akira Mochizuki [d]

[a] Toray Research Center, Inc., 3-3-7 Sonoyama, Otsu, Shiga 520-8567, Japan
[b] Himeji Institute of Technology, University of Hyogo, Kamigori, 678-1297 Hyogo, Japan
[c] Institute of Multidisciplinary Research for Advanced Materials, Tohoku University, 2-1-1, Katahira, Aoba-ku, Sendai 980-8577, Japan
[d] Department of Bio-Medical Engineering, School of High-Technology for Human Welfare, Tokai University, Nishino 317, Numazu, Shizuoka 410-0395, Japan

ARTICLE INFO

Article history:
Received 8 July 2009
Received in revised form
11 October 2009
Accepted 15 October 2009
Available online 21 October 2009

Keywords:
Network structures and dynamics
^{13}C NMR
Suppressed or recovered intensities (SRI) analysis

ABSTRACT

We recorded temperature-dependent high-resolution ^{13}C NMR spectra of dry and swollen poly(-acrylate)s [poly(2-methoxyethyl acrylate) (PMEA), poly(2-hydroxyethyl methacrylate) (PHEMA), and poly(tetrahydrofurfuryl acrylate) (PTHFA)] by dipolar decoupled-magic angle spinning (DD-MAS) and cross-polarization-magic angle spinning (CP-MAS) methods, to gain insight into their network structures and dynamics. Suppressed or recovered intensities (SRI) analysis of ^{13}C CP-MAS and DD-MAS NMR was successfully utilized, to reveal portions of dry and swollen polymers which undergo fast and slow motions with fluctuation frequencies in the order of 10^8 Hz and 10^4–10^5 Hz, respectively. Fast isotropic motions with frequency higher than 10^8 Hz at ambient temperature were located to the portions in which ^{13}C CP-MAS NMR signals of swollen PMEA were selectively suppressed. In contrast, low-frequency motion was identified to the portions in which ^{13}C DD-MAS (and CP-MAS) signals are most suppressed at the characteristic suppression temperature(s) T_s. Network of PMEA gels (containing 7 wt% of water) turns out to be formed by partial association of backbones only, as manifested from their T_s gradient at lowered temperature, whereas networks of PHEMA (containing 40 wt% of water) and PTHFA (9 wt% of water) gels are tightly formed through mutual inter-chain associations of both backbones and side-chains, as viewed from the raised T_s values for both near at ambient temperature. It is also interesting to note that flexibility of gel network (PMEA > PTHFA > PHEMA) characterized by the suppression temperature T_s (PMEA < PTHFA < PHEMA) is well related with a characteristic parameter for biocompatibility such as the production of TAT (thrombin–antithrombin III complex) as a marker of activation of the coagulation system.

1. Introduction

Much interest has been paid to develop a variety of hydrated polymeric materials, which swell in water but do not dissolve, as biocompatible materials used for contact lens, drug delivery system, surface-coating material for medically used devices, etc. [1,2]. To this end, Tanaka et al. demonstrated that poly(2-methoxyethyl acrylate) (PMEA) (I) surface exhibits excellent blood compatibility [3] (Scheme 1).

Indeed, protein and cellular adhesion onto a surface of PMEA are substantially limited as compared with those of analogous poly(acrylate)s such as poly(hydroxyethyl methacrylate) (PHEMA) (II), poly(tetrahydrofurfuryl acrylate) (PTHFA) (III) [4,5], and poly(n-butyl acrylate) (PBA) [6–9]. In fact, PMEA is now widely used for a variety of medical applications [10].

Such excellent performance of PMEA was proposed to arise from specific water structures in the polymer as viewed from comparative studies on DSC measurements and blood compatibility [11–14]. The proposed freezing bound water, defined as having cold crystallization from −50 to −20 °C as estimated by DSC measurement, was shown to play a very important role in expressing the good blood compatibility [14]. It seems to be not always straightforward, however, to attempt characterization of swollen or hydrated structure in terms of solvent water molecules present in interstice

* Corresponding author. Tel: +81 77 533 8617; fax: +81 77 533 8696.
** Corresponding author. Tel./fax: +81 78 856 2876.
E-mail addresses: yuuko_miwa@trc.toray.co.jp (Y. Miwa), hsaito@siren.ocn.ne.jp (H. Saitô).

0032-3861/$ – see front matter © 2009 Elsevier Ltd. All rights reserved.
doi:10.1016/j.polymer.2009.10.037

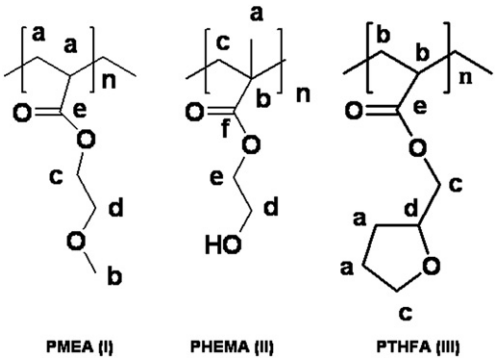

Scheme 1.

of polymer network at ambient temperature, based on DSC measurements performed at lower temperatures.

As an alternative approach, measurements of water ^{1}H, ^{2}H or ^{17}O spin–lattice relaxation times (T_1) and spin–spin relaxation times (T_2) have been, in many instances, performed to characterize states of water molecules present in hydrogels [15–20] as well as those in biological tissues [21–24]. The presence of two or three kinds of water molecules, free, bound or intermediate water molecules, could be postulated for interpretation of such T_1 (or T_2) data

$$1/T_1 = a(1/T_{1\text{free}}) + b(1/T_{1\text{bound}}) + c(1/T_{1\text{intermediate}}) \quad (1)$$

where corresponding fractions, a, b, and c are normalized as: $a + b + c = 1$. It is not easy, however, to evaluate accurately such four to six parameters, including two to three respective T_1 (or T_2) values as well as their relative proportions, a, b or c, from a single set of experiment, although relaxation measurements at several different Larmor frequencies are highly recommended [25]. Still, it is very difficult to evaluate these parameters, even though some of such relative contributions were estimated by DSC data at low temperature [13–16]. As questioned by Roorda [26], there appears no justification to separate properly such water structures at ambient temperature into two or three components by extrapolation of the DSC data taken at very low temperatures. Therefore, these approaches seem to be not always reliable as a means to characterize a variety of hydrogels for further development of biocompatible materials.

Instead, characterization of hydrated polymers or hydrogels, based on well-resolved individual ^{13}C NMR signals of particular sites by high-resolution ^{13}C solution or solid-state NMR, could provide more direct and reliable information about their structures and dynamics, as compared with the above-mentioned indirect approach using solvent molecules [27–30]. This is because such network structure and dynamics of polymer chains might play important role to regulate the so-called "water structures". Nevertheless, it is emphasized here that spin–lattice relaxation time T_1, sensitive to fast motions, of PHEMA and other type of hydrogels including polysaccharide gels was unchanged in the presence or absence of cross-linked portion, whereas line-widths characterized by spin–spin relaxation time T_2, sensitive to low frequency motions, were substantially broadened by resulting slow motions [27–30].

Therefore, it is expected that such T_2-based ^{13}C NMR measurements could provide insight into gel structure and dynamics. Indeed, single pulse, dipolar decoupled-magic angle spinning (DD-MAS) yields well-resolved ^{13}C NMR signals due to the presence of high frequency motions of swollen flexible, polymer chains ($>10^8$ Hz) [27–30], although the corresponding CP-MAS spectra were consequently suppressed. In contrast, ^{13}C NMR signals from inflexible chains including cross-linked region could be recorded by cross-polarization magic angle-spinning (CP-MAS) method. In such case, it is emphasized that such low frequency motion in such polymer chains, if any, could be conveniently examined by suppressed peak intensities as described below. Moreover, it has been shown that low frequency motions with frequencies of 10^4 Hz–10^5 Hz play an essential role at either active center or surface areas for globular and membrane proteins at physiological temperature [33–35]. For this purpose, we examined suppressed or recovered intensities (SRI) plots of DD-MAS and CP-MAS spectra, caused by interference or escape of incoherent fluctuation frequency with coherent frequency of proton decoupling or magic angle spinning, respectively, to reveal occurrence of such low frequency motions [31–35].

Here, we carefully compared ^{13}C DD-MAS and CP-MAS NMR spectra of PMEA (containing 7 wt% of water), PHEMA (containing 40 wt% of water) and PTHFA (containing 9 wt% of water), recorded at temperatures between −80 °C (or −70 °C) and 37 °C, to gain insight into their network structures and chain dynamics. It turned out that PMEA surface is very flexible (with fluctuation frequency being 10^8 Hz) at ambient temperature (37 °C) as viewed from their suppressed signals from the CP-MAS. In addition, low frequency motions persist in the side-chain moieties of PMEA even at low temperatures −40 to −50 °C, as judged by the suppression temperature T_s from analysis of SRI plots, as compared with those of PTHFA (0 to −10 °C) and PHEMA (~37 °C). Indeed, network structure of swollen PMEA is formed by hydrophobic association of backbone only. In contrast, PHEMA molecule is tightly held together through associations of both side-chains and backbones, resulting in prevention of fast and slow fluctuation motions as manifested from the suppression temperature T_s near at ambient temperature.

2. ^{13}C suppressed or recovered intensities (SRI) against fluctuation frequencies

2.1. Static or high frequency fluctuation

The maximum ^{13}C CP-MAS NMR intensity (S) is available from samples of static or nearly static state (I_a) usually achieved in frozen state, if the contact time for this experiment is appropriately chosen. These peaks are decreased together with increased fluctuation frequencies, and finally disappear when isotropic, random fluctuation motions with frequencies $> 10^8$ Hz are dominant (see the solid curve in the SRI plots of CP-MAS experiment in Fig. 1). The maximum ^{13}C intensity (S) for DD-MAS NMR spectra, on the other hand, is achieved for samples at a temperature above the glass transition or in solution, undergoing isotropic fluctuation motions (see the curve III_b). Such intensity changes could be modified in the presence of any sort of molecular motions.

The range of the fluctuation frequencies were divided into the following three regions, static (I_a or I_b), slow (II_a or II_b), and high frequency (III_a or III_b) regions. In the presence of slow fluctuation motions, the peak intensities can be modified as shown by the dotted lines (II_a' or II'_b). In the nearly static region at low temperatures, the peak-intensities could be also changed into the dotted lines I_a' or I_b', due to persistent molecular motions in the glassy state, depending upon efficiency of cross-polarization or their T_1 values. In such case, the observed peak intensity $I(t)$ for DD-MAS spectra could be modified depending upon the ratio t/T_1 [36],

$$I(t) = I(\infty)[1 - \exp(-t/T_1)] \quad (2)$$

where t and T_1 show the pulse repetition and ^{13}C spin–lattice relaxation times, respectively, and $I(\infty)$ is the peak intensity

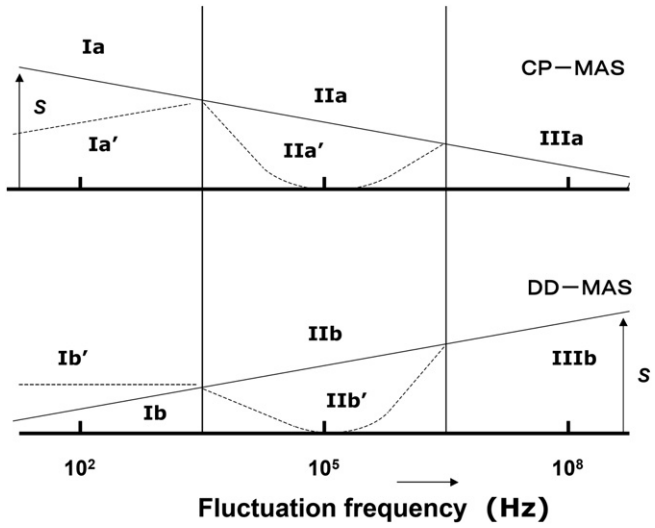

Fig. 1. Expected SRI plots for ^{13}C CP-MAS (top) and DD-MAS (bottom) NMR peak-intensities (solid lines) against fluctuation frequency (Hz). The range of the fluctuation frequencies were divided into the following three regions, static (I_a or I_b), slow (II_a or II_b), and high frequency (III_a or III_b) regions. The maximum intensities are given by S. In the presence of slow fluctuation motions, the peak-intensities can be expressed by the dotted lines (II_a′ or II'_b). In the nearly static region, the peak-intensities could be changed into the dotted lines I_a′ or I_b′, depending upon efficiency of cross-polarization or T_1 values (see the text).

at $t \gg T_1$. It is, therefore, essential to record both ^{13}C CP- and DD-MAS NMR spectra, to gain insight into structures and dynamics of a variety of hydrogel.

2.2. Low frequency fluctuations

Such an intensity change could be further modified in the presence of low-frequency fluctuation in the order of 10^4–10^5 Hz, because such incoherent frequencies from random motions can interfere with coherent frequencies of proton decoupling or magic angle spinning [31,32], leading to failure of attempted peak narrowing for high-resolution NMR (see the dotted curves II_a′ or II_b′ instead of the solid lines in Fig. 1). In such case, ^{13}C NMR line width $1/\pi T_2{}^C$ of polymer chains can be dominantly determined by the following second or third terms, instead of the first static component [37],

$$1/T_2{}^C = (1/T_2{}^C)^S + (1/T_2{}^C)^M{}_{DD} + (1/T_2{}^C)^M{}_{CS} \quad (3)$$

where $(1/T_2{}^C)^S$ is the transverse component due to static C–H dipolar interactions, and $(1/T_2{}^C)^M{}_{DD}$ and $(1/T_2{}^C)^M{}_{CS}$ are the transverse components due to the fluctuation of dipolar and chemical shift interactions in the presence of internal fluctuation motions, respectively. The latter two terms are given as a function of the correlation time τ_c by [31,32],

$$(1/T_2{}^C)^M{}_{DD} = \Sigma(4\gamma_I{}^2\gamma_S{}^2\hbar^2/15r^6)I(I+1)(\tau_c/(1+\omega_I{}^2\tau_c{}^2)) \quad (4)$$

$$(1/T_2{}^C)^M{}_{CS} = (\omega_0^2\delta^2\eta^2/45)(\tau_c/(1+4\omega_r{}^2\tau_c{}^2)+2\tau_c/(1+\omega_r{}^2\tau_c{}^2)) \quad (5)$$

Here, γ_I and γ_S are the gyromagnetic ratios of I (proton) and S (carbon) nuclei, respectively, and r is the internuclear distance between spins I (and also spin number) and S. ω_0 and ω_I are the carbon resonance frequency and the amplitude of the proton decoupling RF field, respectively. ω_r is the rate of spinner rotation. δ is the chemical shift anisotropy and η is the asymmetric parameter of the chemical shift tensor. Thus, the line broadening occurs when incoherent fluctuation frequency is very close to the coherent amplitude of proton decoupling ω_I (10^5 Hz; Eq. (4)) or ω_r (10^4 Hz; Eq. (5)), as schematically plotted against fluctuation frequency (the dotted lines, II_a′ or II_b′) in Fig. 1. The latter broadening is for the carbonyl or quaternary carbon signal.

The experimental ^{13}C SRI plots for both CP-MAS and DD-MAS spectra are usually expressed against temperature, pH [38], etc., instead of the fluctuation frequency as shown in Fig. 1, however. It is recognized that such fluctuation frequency can be considered to be proportional to temperature, in view of accelerated fluctuation frequencies achieved at elevated temperature. Therefore, the suppression temperature T_s, at which the peak intensity is most suppressed, can be conveniently utilized as a parameter to clarify polymer dynamics of specific sites, depending upon the fluctuation frequency for protonated (10^5 Hz) or unprotonated (10^4 Hz) carbons which can interfere with frequencies of the proton decoupling or magic angle spinning.

3. Materials and methods

PMEA, PHEMA and PTHFA were prepared by radical polymerization of respective monomers, using 2,2′-azobis-isobutyronitril (AIBN) as an initiator [3–5]. These polymers were dissolved in either tetrahydrofuran (THF) or methanol solutions, and purified by precipitation three-times after pouring into hexane and diethyl ether (PMEA and PHEMA) or diisopropylether (PTHFA), yielding viscous gum (PMEA and PTHFA) and white powder (PHEMA). The apparent weight average molecular weights (M_w) of PMEA, PHEMA and PTHFA were 85,000,75,000 and 60400, respectively [39] (by size-exclusion chromatograpy, polystyrene standard; as to inherent problems, see refs [40,41]).

The fully hydrated polymers were prepared by soaking the polymers thus prepared in deuterium oxide using an ultrasonic generator for 18–35 days, followed by wiping out with filter paper to remove excess water on the surface, weighing quickly (W_1), and drying at 110 °C for 4 h in vacuum oven, until the weight (W_0) became constant. The water content (W_C) of the polymers was calculated by

$$W_C(\mathrm{wt\%}) = (W_1 - W_0)/W_1 \times 100, \quad (6)$$

where W_0 and W_1 are the weights of the dried and the hydrated samples, respectively.

^{13}C NMR spectra were recorded on a Chemagnetics CMX 300 NMR spectrometer operating at 7.05 T at temperatures −80 °C or −70 °C to 37 °C, by both CP-MAS and DD-MAS methods. ^{13}C NMR spectra were acquired by starting measurements from the low temperature at −80 °C or −70 °C and changing temperatures by always heating the sample to arrive at desired temperature to avoid ambiguity owing to hysteresis effect. Samples were tightly sealed in a sample rotor during NMR measurements. Magic angle frequency was set to 3.5 kHz. The 90° pulse, contact time, and recycle time were 4.5 μs, 1.5 ms, and 7 s, respectively. At desired temperatures, sample was maintained for 20 min before NMR measurements.^{13}C spin–lattice relaxation times (T_1s) of PMEA, PTHFA and PHEMA at ambient temperature were determined by the progressive saturation method, based on a plot of log [$I(\infty) - I(t)$] against t from Eq. (2) [42].

4. Results

We found that ^{13}C spin–lattice relaxation times of polyacrylates are less than 1 s, as far as their protonated, side-chain carbons are

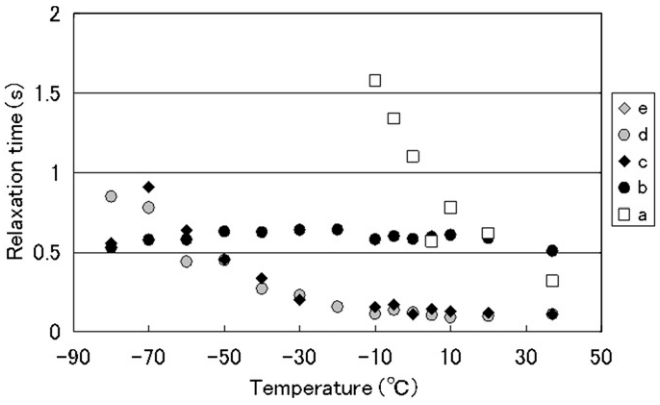

Fig. 2. ^{13}C spin–lattice relaxation times of swollen PMEA (7 wt%) against temperatures. Symbols a–e denote the carbon atoms in the Scheme.

concerned, as demonstrated in the case of swollen PMEA as shown in Fig. 2. In such case, therefore, almost full peak intensities of protonated, side-chain carbons can be expected from Eq. (2) for the individual DD-MAS NMR peaks under the present experimental condition.

Fig. 3A and B show the ^{13}C CP-MAS and DD-MAS NMR spectra of dry PMEA at temperatures between −80 °C and 37 °C, respectively. The maximum NMR peak-intensities were available from the CP-MAS and DD-MAS spectra recorded at the lowest (−80 °C) and highest temperatures (37 °C), respectively, consistent with the expected SRI plots as illustrated in Fig. 1. In a similar manner, Fig. 4 illustrates the ^{13}C CP-MAS and DD-MAS NMR spectra of PMEA hydrogel containing 7 wt% water. Fig. 5A and B illustrate the resulting SRI plots of ^{13}C DD-MAS NMR spectra for dry and swollen PMEA, respectively. Obviously, the suppression temperatures T_S of hydrogel, at which their respective peaks are most suppressed, are shifted to lower temperature sides as compared with those of dry sample (see also Table 1), although the extent of such shifts differ substantially among the signals of respective sites (T_S gradient). On the contrary, the corresponding SRI plots from CP-MAS NMR spectra are rather obscured because of the drastic intensity changes due to differential efficiency of cross-polarization at lower temperature side and also extremely suppressed intensities at raised temperature, as shown in Fig. 6. Therefore, the suppression temperatures T_S's, in these cases, are more clearly seen from the DD-MAS spectra than the CP-MAS spectra.

Fig. 7A and B show the ^{13}C CP-MAS and DD-MAS NMR spectra of swollen (containing 40 wt% water) PHEMA, respectively, recorded at temperatures between −70 °C and 37 °C. Further, the maximum CP-MAS peak-intensities of PHEMA containing 40 wt% water were achieved at −30 °C (Fig. 8A), although the maximum DD-MAS NMR intensities were seen at −30 °C and 0 °C for the side-chain and backbone (Fig. 8B), respectively. Fig. 9 illustrates the SRI plots of ^{13}C DD-MAS NMR spectra for dry (A) and swollen (B) PHEMA against temperature. The corresponding SRI plots from the CP-MAS NMR spectra are shown in Fig. 10. Further, Fig. 11 illustrates similar SRI plots of ^{13}C DD-MAS spectra for swollen PTHFA containing 9 wt% of water against temperature. Corresponding SRI plots of the ^{13}C CP-MAS NMR spectra are also shown in Fig. 12.

5. Discussion

5.1. Network structures

The most distinct feature in the SRI plots among the hydrogels of PMEA, PHEMA and PTHFA is that the intensities of their individual peaks were varied with temperatures quite different ways (Figs. 5, 8 and 11). The suppression temperatures T_S's for the backbone, side-chain, and the terminal methyl carbons for PMEA hydrogel are −10 °C, −30 °C and −40 °C, and −50 °C, respectively (Table 1). In contrast, the corresponding T_S's for the backbone and side-chain of PTHFA hydrogel are 30 °C and 0 °C, respectively and those of PHEMA hydrogen are ≥ 37 °C and ∼37 °C, respectively. In short, the suppression temperature is elevated in the following order: PMEA < PTHFA < PHEMA. Such distinction can be ascribed to the presence of two types of gel networks, as schematically drawn in Fig. 13. PMEA hydrogel could be cross-linked by unswollen

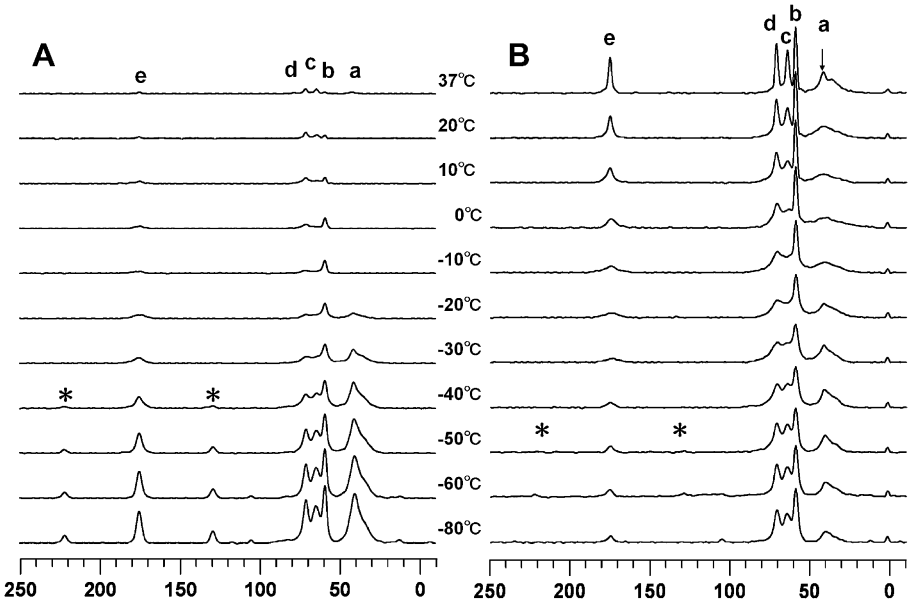

Fig. 3. ^{13}C CP-MAS (A) and DD-MAS (B) NMR spectra of dry PMEA recorded at various temperatures. The alphabetical letters at the top of peaks are ascribed to the individual carbon sites for PMEA (see the scheme). Note the peak intensity *a* (arrow) in the DD-MAS NMR spectra is more evident at higher temperatures. Asterisk denotes spinning sideband.

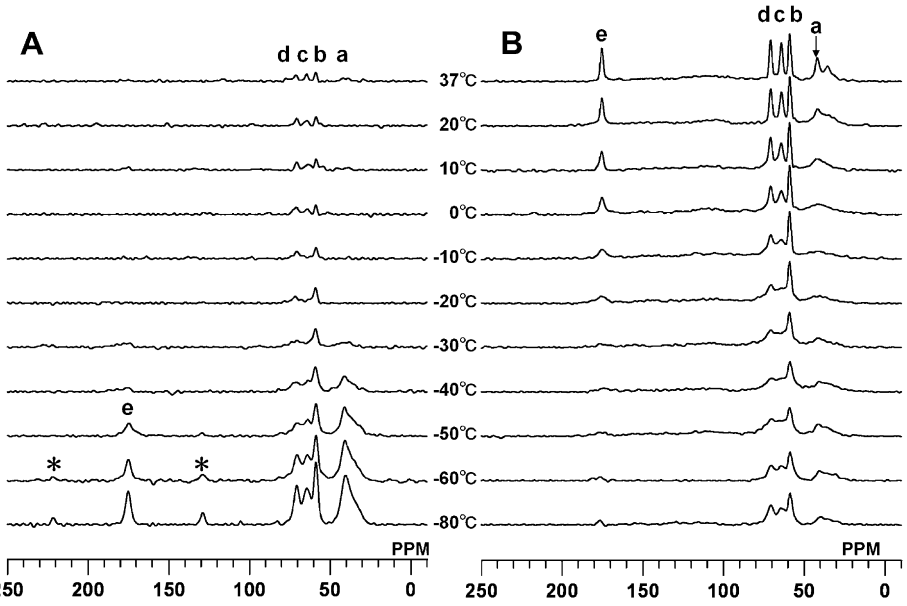

Fig. 4. ^{13}C CP-MAS (A) and DD-MAS (B) NMR spectra of PMEA containing 7 wt% water, recorded at various temperatures. The alphabetical letters at the top of peaks are ascribed to the individual carbon sites for PMEA (see the scheme). Note the peak intensity *a* (arrows) in the DD-MAS NMR spectra is more evident at higher temperatures.

hydrophobic cores of associated backbones, leaving free side-chains undergoing rapid fluctuation motions at ambient temperature (Fig. 13A). In contrast, the gel networks of PHEMA and PTHFA could be more tightly formed by the hydrophobic cores of the associated backbones, and also the side-chains through either hydrogen bonding or entanglement of bulky tetrahydrofurfuryl side-chains (as shown by the circles in Fig. 13B), respectively, as judged by their simultaneous intensities-changes as well as raised T_s's as schematically shown in Fig. 13B.

Naturally, such network structures may be also persistent in unswollen, dry PMEA polymer of glassy state, as seen from their SRI plots (Fig. 5A), even if their suppression temperatures T_s's are shifted to higher temperature in the absence of water molecules as a lubricant. The ^{13}C DD-MAS NMR signals of dry PMEA are more intense than those of PMEA hydrogel at −80 °C (Figs. 3 and 4). Further, it is surprising that the intense ^{13}C DD-MAS NMR of dry PHEMA signals are visible even at −70 °C, far below its glass transition temperature at 35°–109 °C [43] (Fig. 7). These results can be justified, however, if the spin–lattice relaxation times T_1's are not always prolonged even at such low temperature for glassy polymers, in contrast to those of crystalline samples such as cellulose or polyethylene, due to the presence of relaxation pathway via C–H dipolar interactions with rotating α-methyl group or the side-chain groups. Accordingly, its T_1 remains, at most, in the order of 100 ms [44]. As a result, resultant ^{13}C peak-intensities in this region could be expressed by the dotted line I_b', rather than the solid line I_b mentioned above (Fig. 1).

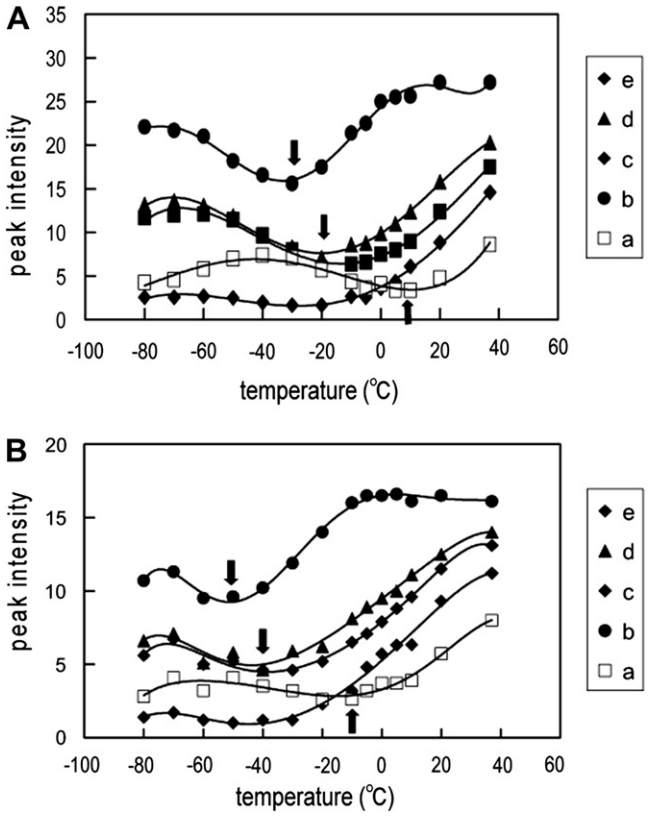

Fig. 5. The SRI plots of the ^{13}C DD-MAS NMR spectra for dry (A) and swollen (containing 7 wt% water) (B) PMEA, respectively, against temperature. Suppression temperatures T_S at which respective peaks are most reduced are shown by the arrows.

Table 1
The suppressed temperature T_s at which ^{13}C NMR peak-intensities are most suppressed in the presence of slow motions (°C).

	PMEA		PTHFA	PHEMA
	Dry	Containing 7% D_2O	Containing 9% D_2O	Containing 40% D_2O
Backbone	7	−10	30	≥37
$COOCH_2CH_2$ (or –OH)[a] or $COOCH_2$furfuryl[b]	−12	−30	0	≈37
$COOCH_2CH_2$ (or –OH)[a]	−20	−40		≈37
$COOCH_2CH_2OCH_3$ (or OH)[a] or $COOCH_2$furfuryl[c]	−30	−50	−10	≥37
$COOCH_2CH_2OCH_3$ (or –OH)[a]	−20	−40		≥37

[a] PHEMA.
[b] PTHFA.
[c] From peak d.

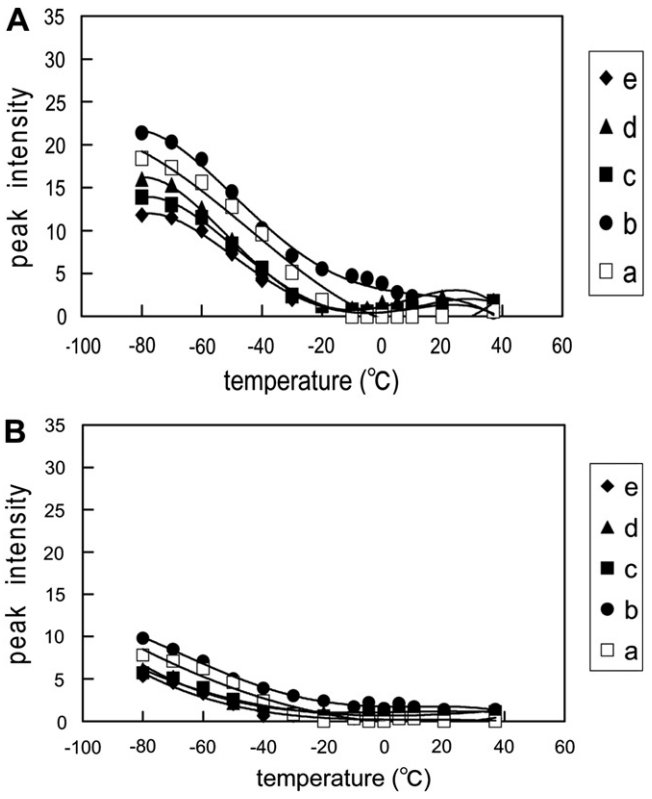

Fig. 6. The SRI plots for dry (A) and swollen (B) PMEA available from their CP-MAS NMR spectra against temperature.

5.2. Chain dynamics

5.2.1. Fast dynamics

Fully swollen polymer chains in hydrogels are generally very flexible to give well-resolved ^{13}C NMR signals visible even by solution NMR spectrometer [27,28,30], although ^{13}C NMR signals of polymer chains located in the vicinity or involved in the cross-linked regions are suppressed as viewed from solution or DD-MAS NMR spectra [27–30,33]. Although the spin–lattice relaxation times T_1's are generally appropriate means to examine dynamics of such flexible portions, they are not always sensitive to the current gel dynamics, because their T_1 values lie at their minimum. Instead, distribution of correlation times as in log-χ^2 distribution [45] results in line broadened signals in gel samples [27,28].

5.2.2. Slow dynamics, PMEA

The presence of the physically cross-linked portion of hydrogel network, however, results in the partially suppressed peak-intensities in the backbone signals in the DD-MAS spectra of PMEA gel (Fig. 4) as denoted by the peak *a* at the highest field region, although their side-chains undergo rapid fluctuation motion with frequency higher than 10^8 Hz at ambient temperature (Table 2). Such suppressed ^{13}C DD-MAS NMR peaks can be explained by shortened spin–spin relaxation time T_2^C under the condition of either proton decoupling or magic angle spinning due to failure of such attempted high-resolution NMR spectra, when fluctuation frequency interferes with frequency of proton-decoupling or magic angle spinning (10^4–10^5 Hz; Table 2). As demonstrated in Fig. 5B and summarized in Table 1, the lowest, suppression temperature T_s for PMEA gel is -50 °C corresponding to the motion of the terminal moiety of the side-chains which are surrounded by frozen water.

Interestingly, the suppression temperature T_s was made lower together with the sites in the side-chains in the following order, as demonstrated in Figs. 5, 8, and 11 and summarized in Table 1.

$$\mathrm{COO\underline{C}H_2CH_2OCH_3} > \mathrm{\underline{C}OOCH_2CH_2OCH_3} \sim \mathrm{COOCH_2\underline{C}H_2OCH_3} > \mathrm{COOCH_2CH_2O\underline{C}H_3}. \quad (7)$$

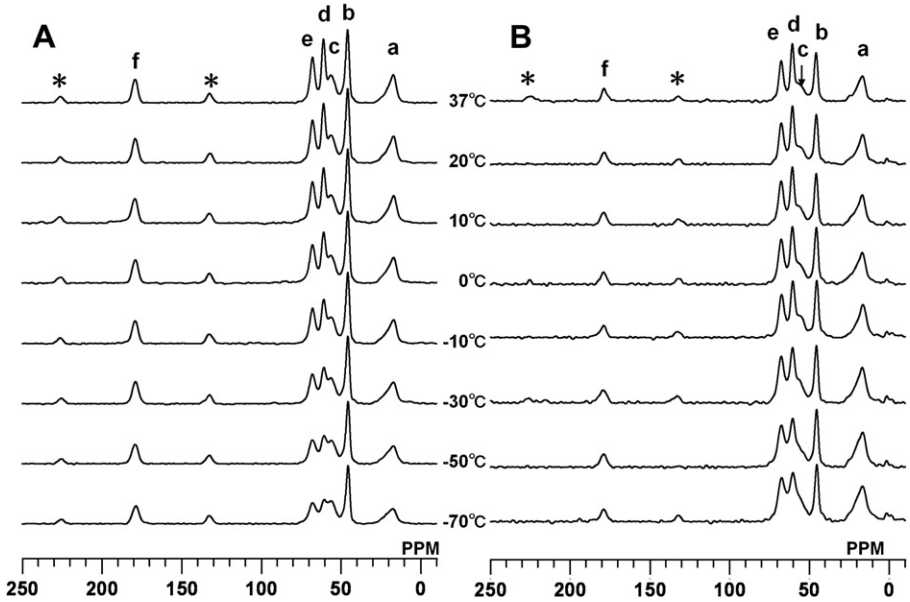

Fig. 7. ^{13}C CP-MAS (A) and DD-MAS (B) NMR spectra of dry PHEMA, recorded at various temperatures. The alphabetical letters at the top of peaks are ascribed to the individual carbon sites for PHEMA (see the scheme). Note the peak intensity *b* and *c* (arrow) in the DD-MAS NMR spectra at higher temperatures.

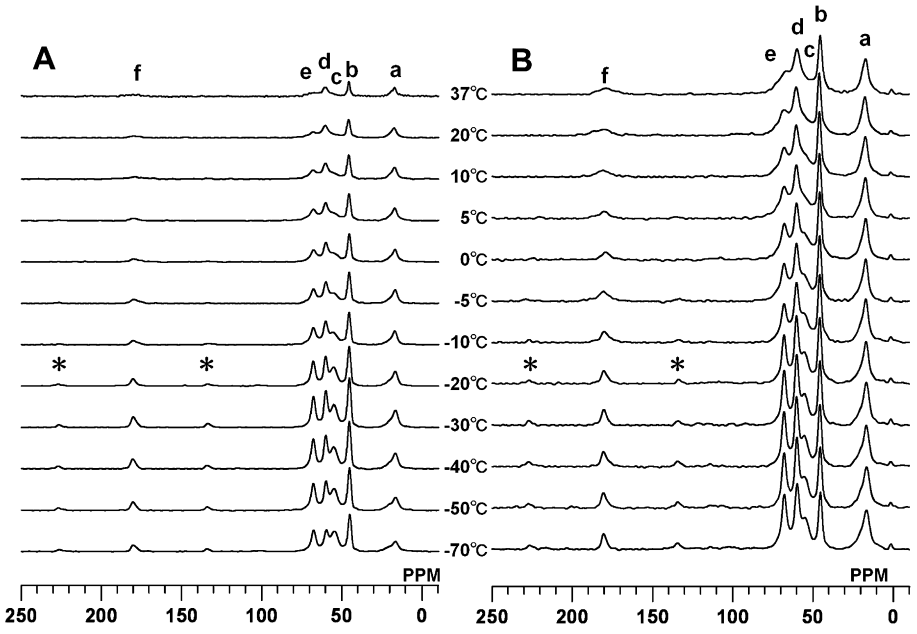

Fig. 8. ^{13}C CP-MAS (A) and DD-MAS (B) NMR spectra of PHEMA containing 40 wt% water recorded at various temperatures. The alphabetical letters at the top of peaks are ascribed to the individual carbon sites for PHEMA (see the scheme).

Among the last protonated three carbon sites in Eq. (7) indicated by the face underlined, the respective correlation times (or fluctuation frequencies) may be modified in the presence of the following internal rotation around the single bonds: –COO–CH_2–CH_2–O–CH_3. If internal rotation occurs at a rate τ_i^{-1} around an axis whose reorientation is described by a correlation time τ_m, the effective local correlation time τ_c is given by superposition of overall τ_i and internal motions τ_m [46–48]

$$\tau_c = (1/4)(3\cos^2\theta - 1)2\tau_m + (3/4)(\sin^2 2\theta + \sin^4\theta) \times (1/\tau_m + 1/\tau_i)^{-1} \quad (8)$$

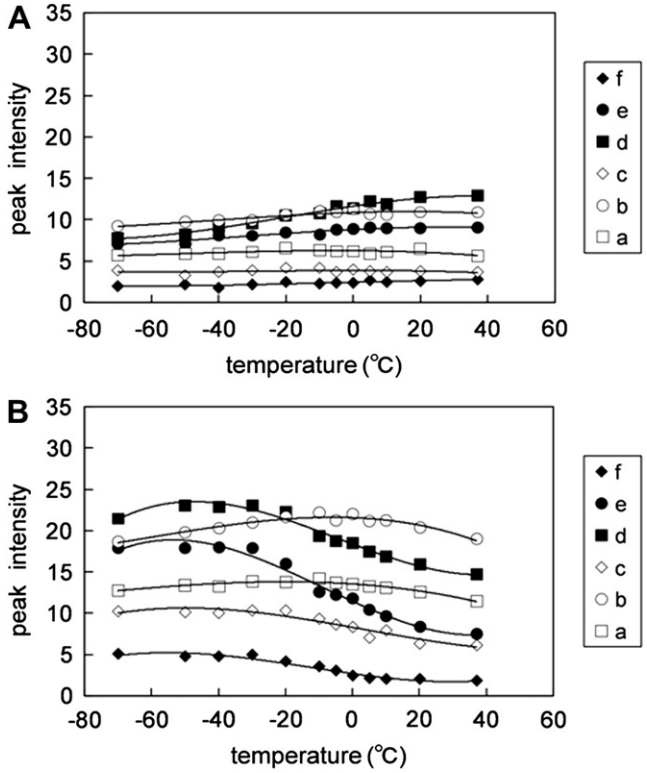

Fig. 9. The SRI plots of the ^{13}C DD-MAS NMR for dry (A) and swollen (containing 40 wt% water) (B) PHEMA against temperature.

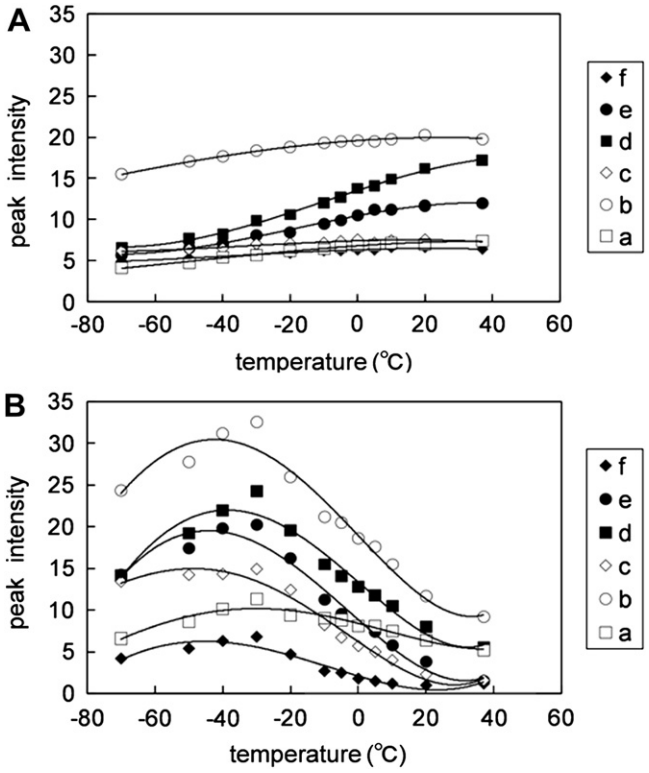

Fig. 10. The SRI plots of the ^{13}C CP-MAS NMR spectra for dry (A) and swollen (B) PHEMA against temperature.

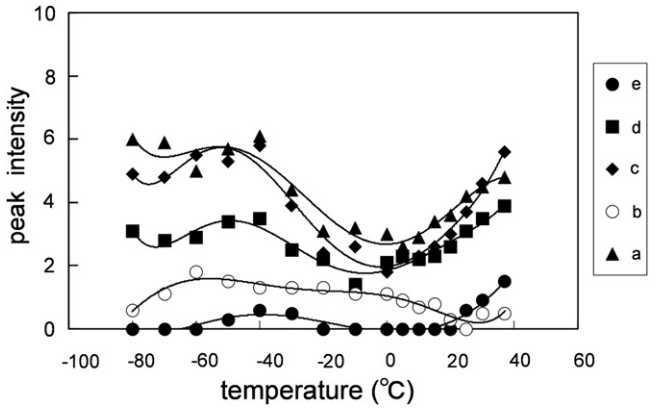

Fig. 11. The SRI plots of the ^{13}C DD-MAS NMR for PTHFA hydrogel containing 9 wt% water against temperature.

where θ is the angle between the rotation axis and C–H bond axis. Because θ is equal to the tetrahedral angle,

$$\tau_c = 0.11\tau_m + 0.89(1/\tau_m + 1/\tau_i)^{-1} \quad (9)$$

If $\tau_i << \tau_m$ as in the case of OCH_3 group in the solid, Eq. (9) is described by $\tau_c = 0.11\tau_m$.

When several internal rotations are present as in the present situation, the resultant local motions may be derived in analogous fashion. Starting with the largest rigid part of the molecule, the motion of the *n*th bond axis results from the motion of the $(n-1)$th axis, so on. For instance two internal rotations with time constant τ_i and τ_j, the effective correlation time could be described by $\tau_c = 0.01\tau_m$, when $\tau_i << \tau_m$ and $\tau_j << \tau_m$. This consideration shows that the fluctuation frequency $(1/\tau_c)$ is shifted to lower frequency and subsequently to the lower T_s, depending upon the number of internal rotations.

5.2.3. Slow dynamics, PHEMA and PTHFA

The network structures of PHEMA and PTHFA hydrogels are far from flexible at ambient temperature, as viewed from the increased T_s and intense CP-MAS NMR. Indeed, the fluctuation frequencies of the side-chains for PHEMA and PTHFA gels are in the order of 10^5 and 10^8 Hz at ambient temperature, although those of the backbone moiety are 10^5 and $\leq 10^5$ Hz, respectively (Table 2).

The intensity maximum in the ^{13}C CP-MAS NMR spectra of PHEMA hydrogel is seen at the temperature −30 °C rather than at −70 °C of the lowest temperatures studied (Figs. 8A and 10B), although there appears no such maximum in dry sample (Figs. 7A and 10A). This is in contrast to the cases of dry and fully hydrated PMEA and PTHFA, in which the maximum peak-intensities of the SRI plots from CP-MAS spectra are always achieved at the lowest temperature studied, as far as the condition for the most efficient cross-polarization is taken into account. It is also interesting to note from the SRI plot of PHEMA gel based on the DD-MAS spectra (Fig. 10A) that the peak-intensities for the backbone and side-chain carbon signals tend to decrease by raising the temperature from −20 °C to ambient temperature, by acquisition of low-frequency fluctuation motions with frequency in the order of 10^4–10^5 Hz. Indeed, such changes are more significant in the side-chain hydroxyethyl carbons than the backbone carbon signals.

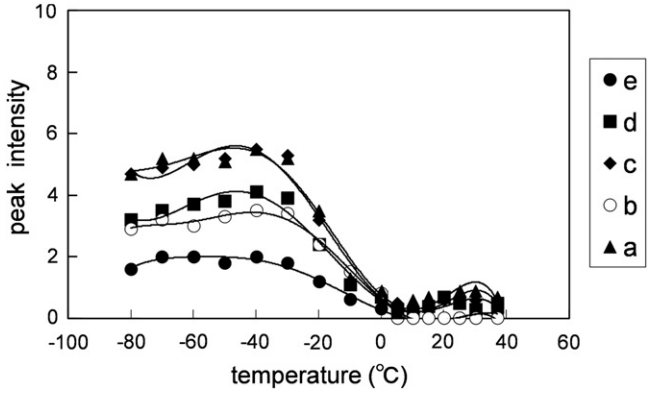

Fig. 12. SRI plots of the ^{13}C CP-MSS NMR spectra for swollen PTHFA against temperature.

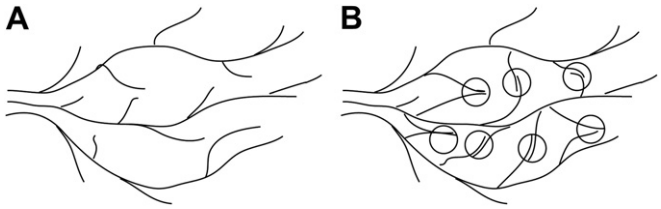

Fig. 13. Schematic representation of the proposed gel network structures for PMEA (A), and PHEMA and PTHFA (B) hydrogels. Cross-links of these gels could be formed by hydrophobic association of the polymer backbones, as illustrated in the left-side portion. The sites, at which side-chains are held together through either hydrogen bonding or entanglement of bulky tetrahydrofurfuryl groups, could be served as additional cross-links, as shown by the circles in the latter.

5.3. Polymer dynamics and water structures in hydrogels

In addition to the presence of fast motions in gel network, identification of low-frequency motion proved to be very important and convenient means to evaluate dynamic property of gel network, even at ambient temperature. Indeed, PMEA hydrogel is very flexible at ambient temperature as characterized by the presence of very fast motions in the backbone and side-chains, whereas PHEMA is least flexible as judged from the suppression temperature T_s at 37 °C (see Table 1). It can be, therefore, concluded that the extent of flexibility in gel network at ambient temperature is well characterized also by the suppression temperature T_s, corresponding to the onset of such slow fluctuation motions. Relative flexibility of these polymer chains can be considered in the following order, PMEA > PTHFA > PHEMA, as judged by their T_s values. In this connection, much attention has been paid to gain insight into water structures present for a variety of biomaterials in relation to its biocompatibility [18,19,49]. This attempt, however, is not always straightforward, because there is a possibility that such structures might be substantially modified by dynamic state of

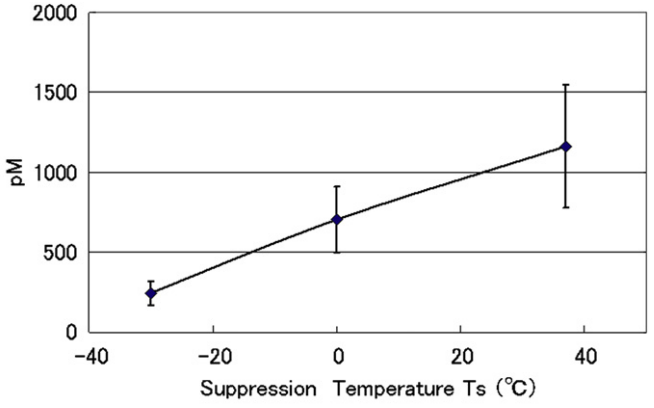

Fig. 14. A plot of produced TAT (thrombin–antithrombin III complex) (pM) [6] against the suppression temperature T_s (°C).

Table 2
Fluctuation frequencies of hydrogels at ambient temperature (37 °C).

	Backbone	Side-chain
PMEA	$>10^8$ Hz	$>10^8$ Hz
PTHFA	10^5 Hz	10^8 Hz
PHEMA	$<10^5$ Hz	$\sim 10^5$ Hz

polymer chains and also polymer networks. Indeed, it is likely that the cold crystalization of water molecules as described above might be triggered by freezing such low frequency motions at the respective temperatures.

Instead, it is interesting to note that the suppression temperature T_s is in parallel with the amount of produced TAT (thrombin–antithrombin III complex) as a measure of biocompatibility activity (Fig. 14). Here, the T_s values were compared for the side-chain carbons neighbored with the COO group (carbons labeled as c in I and III, and e in II) located at the similar positions. This finding implies that good biocompatible material is a polymer undergoing very fast motions at ambient temperature, as judged from the absence of CP-MAS NMR signal at ambient temperature. It is interesting to note that the suppression temperature T_s values can be conveniently utilized as an excellent measure for detailed comparison of such flexibility. It is conceivable that molecular motions of water molecules, which are either coordinated with polymer chains as bound water or in their vicinity might be affected by the presence or absence of fluctuation motions of the terminal moiety of polymer side-chains. Therefore, it is naturally recognized that such differential polymer dynamics might be responsible for concomitant changes in structure and dynamics of surrounding water molecules in the vicinity of constituent polymer network.

Adsorption of proteins to polymer surface is very serious problem for development of a novel material with excellent blood compatibility [3,49–52]. Tanaka et al. [3] demonstrated that PMEA exhibits excellent surface to lead lower platelet adhesion, as manifested from lower denaturation of proteins such as bovine serum albumin and human fibrinogen on its surface as compared with PHEMA. It is easily conceivable that the flexible PMEA surface with side-chains, freely undergoing rapid isotropic fluctuation motions at ambient temperature, might be naturally favorable for preventing any specific interaction with such proteins, because rigidly held network of PHEMA as compared with PMEA could provide more solid surface favorable upon which proteins are able to aggregate, leading to the associated α-helical portion to β-sheet forms as a result of partial denaturation.

5.4. Concluding remarks

We demonstrated that the SRI analysis of ^{13}C DD-MAS NMR for biocompatible hydrogels from poly(acrylate)s provides one invaluable means to yield low frequency dynamics of polymer chains, with emphasis on time-scales of high- (10^8 Hz) and low-frequencies (10^4–10^5 Hz) fluctuations. Such low frequency motion can be characterized by lineshape analysis of ^2H NMR in view of similar frequency dependency [33]. Specific deuteration at specific sites are required for this purpose, however. Water molecules located in interstices of such hydrogels are naturally strongly influenced by such dynamic features of constituent polymers. Direct characterization for such polymer dynamics of hydrogels could be therefore undoubtedly very promising tool for development of biomaterials exhibiting biocompatibility. For this purpose, we emphasize that evaluation of the suppression temperature T_s,at which respective ^{13}C NMR signals are most suppressed in the SRI plots, turns out to be also very useful to locate a portion undergoing low frequency motions in polymer chains at ambient temperature.

Acknowledgements

The authors are grateful to Professor Teiji Tsuruta, University of Tokyo for his valuable advice.

References

[1] Peppas NA, Hilt JZ, Khademhosseini A, Langer R. Adv Mater 2006;18:1345–60.
[2] Jones DS, Lorimer CP, McCoy CP, Gorman SP. J Biomed Mater Res B Appl Biomater 2008;85:417–26.
[3] Tanaka M, Motomura T, Kawada M, Anzai T, Kasori Y, Shiroya T, et al. Biomaterials 2000;21:1471–81.
[4] Tanaka M, Mochizuki A, Motomura T, Shimura K, Ohnishi M, Okahata Y. Colloids Surf A 2001;193:145–52.
[5] Hayashi T, Tanaka M, Yamamoto S, Shimomura M, Hara M. Biointerface 2007;2:119–25.
[6] Mochizuki A, Hatakeyama T, Tomono Y, Tanaka M. J Biomater Sci 2009;20:591–603.
[7] Tanaka M, Mochizuki A, Shiroya T, Motomura T, Shimura K, Onishi M, et al. Colloids Surf A 2002;203:195–204.
[8] Baykut D, Bernet F, Wehrie J, Weichelt K, Schwartz P, Zerkowski HR. Eur J Med Res 2001;30:297–305.
[9] Suhara H, Suwa Y, Nishimura M, Oshiyama H, Yokoyama K, Saito N, et al. Ann Thorac Surg 2001;71:1603–8.
[10] Gunaydin S, Farsak B, Kocakulak M, Sari T, Yorgancioglu C, Zorlutuna Y. Ann Thorac Surg 2002;74:819–24.
[11] Hirota E, Ute K, Uehara M, Kitayama T, Tanaka M, Mochizuki A. J Biomed Mater Res 2006;76:540–50.
[12] Hirota E, Tanaka M, Mochizuki A. J Biomed Mater Res A 2007;81:710–9.
[13] Tanaka M, Mochizuki A, Ishii N, Motomura T, Hatakeyama T. Biomacromolecules 2002;3:36–41.
[14] Tanaka M, Motomura T, Ishii N, Shimura K, Onishi M, Mochizuki A, et al. Poly Interntl 2000;49:1709–13.
[15] Sung YK, Gregonis DE, John MS, Andrade JD. J Appl Polym Sci 1981;26:3719–28.
[16] Hatakeyama T, Yamauchi A, Hatakeyama H. Eur Polym J 1984;20:61–4.
[17] Maquet J, Theveneau H, Djabourov M, Leblond J, Papon P. Polymer 1986;27:1103–10.
[18] Yamada-Nosaka A, Ishikiriyama K, Todoki M, Tanzawa H. J Appl Polym Sci 1990;39:2443–52.
[19] Yamada-Nosaka A, Tanzawa H. J Appl Polym Sci 1991;43:1166–70.
[20] Mathur AM, Scranton AB. Biomaterials 1996;17:547–57.
[21] Cooke R, Wien R. Biophys J 1971;11:1002–17.
[22] Cooke R, Wien R. Ann N Y Acad Sci 1973;204:197–209.
[23] Hazlewood CF, Chang DC, Nichols BL, Woessner DW. Biophys J 1974;14:583–606.
[24] Belton PS, Packer KJ, Sellwood JC. Biochim Biophys Acta 1973;304:56–64.
[25] Finch E, Homer LD. Biophys J 1974;14:907–21.
[26] Roorda W. J Biomater Sci Polym Ed 1994;5:383–95.
[27] Yokota K, Abe A, Hosaka S, Sakai I, Saitô H. Macromolecules 1978;11:95–100.
[28] Saitô H. ACS Symp Ser 1981;150:125–47.
[29] Saitô H. ACS Symp Ser 1992;489:296–310.
[30] Saitô H, Shimizu H, Sakagami T, Tuzi S, Naito A. In: Belton PS, Delgadillo I, Gil AM, Webb GA, editors. Magnetic resonance in food science. Royal Society of Chemistry; 1995. p. 257–71.
[31] Rothwell WP, Waugh J. J Chem Phys 1981;74:2721–32.
[32] Suwelack D, Rothwell WP, Waugh JS. J Chem Phys 1980;73:2559–61.
[33] Saitô H, Ando I, Naito A. Solid state NMR spectroscopy for biopolymers: principles and applications. Springer; 2006.
[34] Saitô H, Tuzi S, Yamaguchi S, Tanio M, Naito A. Biochim Biophys Acta 2000;1460:39–48.
[35] Saitô H, Tuzi S, Tanio M, Naito A. Annu Rep NMR Spectrosc 2002;47:39–108.
[36] Becker ED. High resolution NMR. theory and chemical applications. 3rd ed. Academic Press; 2000.
[37] Naito A, Fukutani A, Uitdehaag M, Tuzi S, Saitô H. J Mol Struct 1998;441:231–41.
[38] Saitô H, Kira A, Arakawa T, Tanio M, Tuzi S, Naito A. Biochim Biophys Acta, in press. doi:10.1016/j.bbamem.2009.06.027.
[39] Tanaka M, Mochizuki A. J Biomed Mater Res 2004;68A:684–95.
[40] Guillaneuf Y, Castignolles P. J Polym Sci A Polym Chem 2008;46:897–911.
[41] Gaborieau M, Graf R, Spiess HW. Macromol Chem Phys 2008;209:2078–86.
[42] Freeman R. A handbook of nuclear magnetic resonance. Longman Scientific & Technical; 1988.
[43] Sung YK, Gregonis DE, Russell GA, Andrade JD. Polymer 1978:1362–3.
[44] Komoroski RA, editor. High resolution NMR spectroscopy of synthetic polymers in bulk. Florida: VCH Publishers; 1986.
[45] Schaefer. J Top Carbon-13 NMR Spectrosc 1974;1:149–208.
[46] Stejskal EO, Gutowsky HS. J Chem Phys 1958;28:388–94.
[47] Woessner DW. J Chem Phys 1962;36:1–4.
[48] Brevard CH, Kintzinger JP, Lehn JM. Tetrahedron 1972;28:2447–60.
[49] Morita S, Tanaka M, Ozaki Y. Langmuir 2007;23:3750–61.
[50] Brash JL, Horbett TA. ACS Sym Ser 1987;343:1–33.
[51] Andrade JD. In: Andrade JD, editor. In surface and interfacial aspects of biomedical polymers. New York: Plenum; 1985. p. 1–80.
[52] Vroman L, Adams AL. J Biomed Mater Res 1969;3:43–67.